

REVIEW PAPER

Composites of conducting polymers and nanoparticles for thin-film-multilayers organic light emitting diodes, organic solar cells and organic gas sensors

Nguyen Nang Dinh[†]

*University of Engineering and Technology, Vietnam National University Hanoi,
144 Xuan Thuy Road, Cau Giay District, Hanoi 10000, Vietnam*

E-mail: [†]dinhnn@vnu.edu.vn

Received 16 December 2024

Accepted for publication 5 February 2025

Published 1 March 2025

Abstract. *In this work we presented a general review on nanostructured composite materials consisting of electrically conducting polymers (CPs) and inorganic nanoparticles used for Organic Light-Emitting Diodes (OLEDs), Solar Cells (OSCs) and Gas Sensors (OGSs). This work gives a topical overview on the synthesis methods and characterization of structure, morphology, and electrical and optical properties as well as performance behaviour of the nanocomposite devices. The analyzed data have demonstrated that the nanostructured composite materials have significantly contributed in the enhancement of both the performance parameters and working time of devices. In this work we concentrated to analyze the most interesting properties of the OLEDs, OSCs and OGSs, such as electro-luminescence, photo-electrical conversion, and gas sensing. This review also presents in general, the discovery of the CPs, some typical CPs and their composites used for fabrication of highly-efficient optoelectronic devices for further applications.*

Keywords: conducting Polymers; nanocomposites; heterojunctions; organic light-emitting diodes (OLEDs); organic solar cells (OSCs); organic gas sensors (OGSs).

Classification numbers: 73.61.Ph; 78.67.Sc; 61.05.C; 07.07.Df; 85.35.-p; 81.07.Pr; 88.40.hj.

1. Introduction

Since the discovery of the electrically conducting polymers (CPs) by Heeger, Shirakawa and MacDiarmid (Nobel prize in Chemistry, 2000), the researches of CPs and CP-based devices have strongly been increasing [1–5]. Similar to inorganic semiconductors, CPs also possess an

energy bandgap - the gap from the highest occupied molecular orbital (HOMO) to the lowest unoccupied molecular orbital (LUMO). When a CP is excited by a sufficient energy, electrons jumped from HOMO to LUMO, and holes appeared in HOMO. This results in the generation of so-called electron-hole-pairs (EHPs) or "excitons". Fabrication of CP-based devices is much easier in comparison with inorganic devices, because thin films of CPs can be deposited by using dip-coating or sol-gel techniques. However, the performance efficiency of the polymeric devices is still low, and it quickly decreased at elevated temperatures, in particular. Embedding inorganic nanoparticles in CPs like metal-oxides, CNTs, quantum dots (QDs), graphene (G), one can produce nanocomposites with enhanced efficiency and long service time of the polymeric devices. There are three main methods used for producing nanocomposites, (i) *in-situ* polymerization: inorganic nano-agents are mixed in monomers then polymerization is taken [6], (ii) solution blending: nano-agents are embedded in polymer solution by carefully stirring, then solvent is removed, intercalated structure remains, resulting in solid nanocomposite [7], and (iii) melt intercalation method: mixtures of polymer and nano-agents are blended in the molten state, followed by annealing to get nanocomposites [8]. The second method is most often used for preparing optoelectronic devices. Comparing with pristine conducting polymers, nanocomposite materials are used in the optoelectronic applications with improved performance efficiency. Next section gives a brief introduction on a group of most used CPs.

2. Electrically conducting polymer – organic semiconducting materials

Inorganic materials often have crystalline structures, whereas polymers and CPs have chain structures from monomers. Bonding in CPs is electronic bonds σ , σ^* and π , π^* . Electrons occupy π levels in the HOMO, similar to energy levels in the valence band of inorganic semiconductors. π^* levels in the LUMO are empty like the energy band in the conducting band of semiconductors. Doping of n- or p-type in a CP is usually carried-out by oxidation or conjugation with another polymer (creating so-called conjugate polymer). Since CPs have quite similar properties of inorganic semiconductors, CPs have also been considered as organic semiconducting materials. Thus, both electronic and optoelectronic devices made from CPs are also based on the p-n junctions, creating organic electronics, such as Organic Light Emitting Diodes (OLED), Organic Solar Cells (OSC), etc. In this section we introduce some typical conducting polymers that are most used: Polyaniline (*PANI*), Polypyrrole (*PPy*), Polyacetylene (*PA*), Poly(3,4- ethylenedioxythiophene):(poly(styrenesulfonate) (*PEDOT-PSS*), Poly[2-methoxy-5-(2'-ethyl-hexyloxy)-1,4-phenylene vinylene] (*MEH-PPV*), and Poly(3-hexylthiophene) (*P3HT*).

2.1. Common structure of conducting polymers

Figure 1 shows the molecular structure of an organic compound "melamine" - $C_3H_6N_6$. Electrons in outermost orbit create covalence bonding σ of two carbon atoms (C-C). Two other electrons create π -bonding. This bonding is rather weak, resulting in instability of the electrons along the polymer chains. However, this is the origin of the larger mobility of the electrical charges in polymers. Conjugate polymers have a larger conductivity compared to standard CPs. Fig. 2 gives the comparison of the conductivities of different materials from metals to semiconductors and isolators. Conjugate polymers possess conductivities lying from 10^{-8} to 10^3 S/cm.

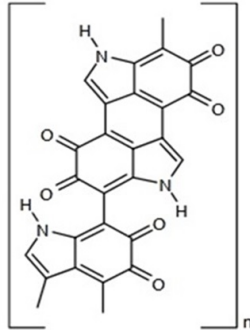


Fig. 1. Molecular structure of melamine, n is the repeatable number of molecules [9].

	Conductivity (S/cm)	Materials
Metallic conductors	10^6	Copper
		Iron
	10^4	Graphite
	10^2	Bismuth
Semi-conductors	10^0	Indium/Antimony
	10^{-2}	Gallium/Arsenic
	10^{-4}	Germanium
	10^{-6}	Silicon
	10^{-8}	
	10^{-10}	
Isolators	10^{-10}	Glass
	10^{-12}	
	10^{-14}	Diamond
	10^{-16}	Sulfur
	10^{-18}	Polyethylene
	10^{-18}	Polystyrene
	10^{-20}	Teflon® Quartz

Fig. 2. Electric conductivity of isolators, semiconductors, and conductive materials [10].

2.2. Polyaniline

The first CP has been known since the publication of Letheby in 1862, when he carried-out a series of chemical reactions on aniline, resulting in formation of polyaniline (PANI) [11]. The work of Letheby can be seen as the first discovery on PANI. Later, PANI has been researched much more carefully, then it is discovered that PANI is also a good conducting polymer. The colour change of PANI occurs due to the oxidation (receiving more electron), PANI changes to blue colour, corresponding to its emeraldine state. This phenomenon was described by Runge in 1834 [12]. When PANI is completely oxidized, it has black colour, corresponding to *pernigraniline* form. The pale reduced form of polyaniline is *leucoemeraldine*, and the green, half-oxidized intermediate is *emeraldine* form. Leucoemeraldine, emeraldine, and pernigraniline are three important oxidation states of PANI. The molecular structures of these three states are shown in Fig. 3.

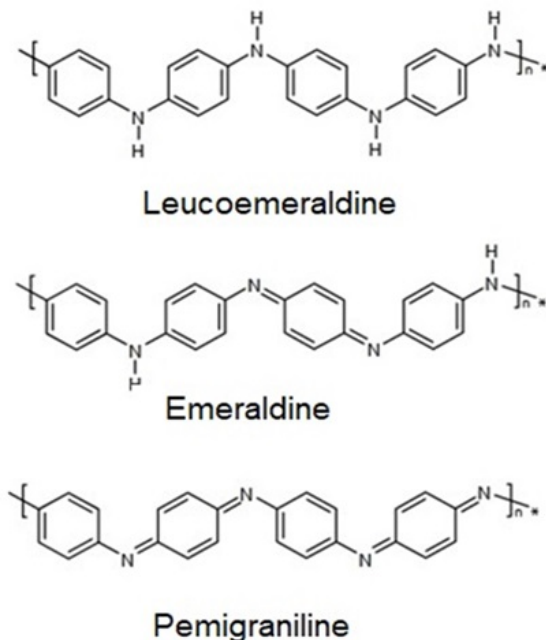


Fig. 3. Polyaniline oxidation states (three different colours) with corresponding their molecular structures [13].

2.3. Poly(3,4-ethylenedioxythiophene) polystyrene sulfonate (PEDOT-PSS)

Poly(3,4-ethylenedioxythiophene) (PEDOT) is combined with polystyrene sulfonate (PSS) to form PEDOT:PSS. It is also a well-known conjugate polymer where PEDOT is a conducting polymer, and PSS is a counter-ion to balance the charge and improve the water solubility and processability of PEDOT. The molecular structure of PEDOT-PSS is described in Fig. 4 [14].

To synthesize PEDOT:PSS, an aqueous solution of PSS is mixed in EDOT monomer with the addition of the solution of sodium persulfate and ferric sulfate. As a result, these reagents initiate the oxidative chemical polymerization of EDOT in water to form PEDOT. The negatively

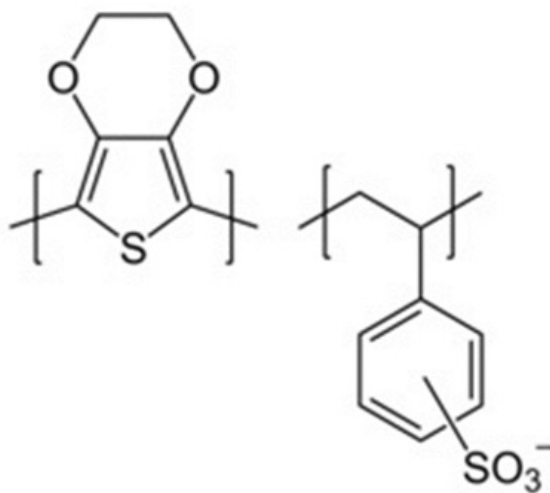


Fig. 4. Molecular structure of PEDOT-PSS [14].

charged sulfonic acid ions help stabilize the positively charged PEDOT ions. PEDOT-PSS are usually used as the hole transport layer (HTL) in OLEDs and OSCs.

2.4. Polyacetylene

The most important period of the discovery process on the CPs is the work on the doping polyacetylene (PA) with the molecular structure shown in Fig. 5.

The most important discovery on the CPs was published in 1977 with an experiment of Heeger, MacDiarmid and Shirakawa on the polyacetylene (PA), its chemical formula is $(C_2H_2)_n$, doped with metallic ions (PA-d). Their articles have been published in 1997 and 2001 [15, 16]. Basing on the theory of solid-state physics and quantum chemistry, the authors have explained the mechanism of the electrical conductance of PA-d. Doping metallic ions in the polymer created new energy level of the carries. In CP carries are not simply electrons or holes, they are electrical complexes, for example, tetrathiafulvalene-tetracyanoquinodimethane [10] which is described in Fig. 6. Among these complexes, phonons are the most important in the CPs. With the published articles on the doping PA, Heeger, Shirakawa and MacDiarmid received Nobel prize in 2001.

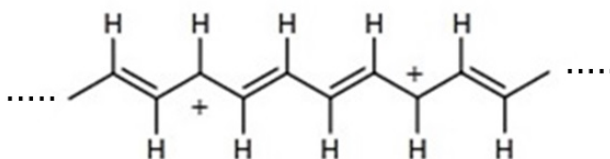


Fig. 5. Molecular structure of polyacetylene [17].

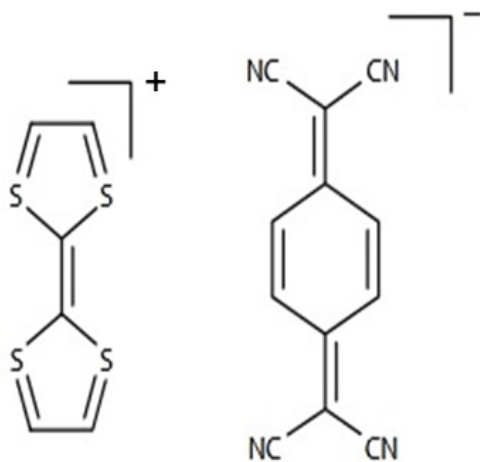


Fig. 6. Tetrathiafulvalene-tetracyanoquinodimethane complex [10].

2.5. Poly[2-methoxy-5-(2'-ethyl-hexyloxy)-1,4-phenylene vinylene] (MEH-PPV)

Molecular structure of MEH-PPV is shown in Fig. 7.

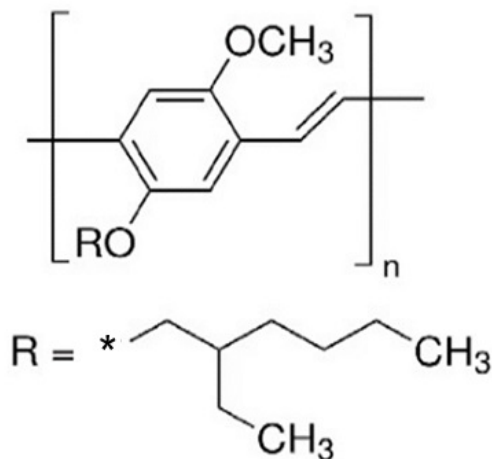


Fig. 7. Molecular structure of MEH-PPV [18].

MEH-PPV is a conjugate polymer which has low molecular weight and hydrophobic characteristic. It is a poly(phenylenevinylene (PPV) derivative with Poly[2-methoxy-5-(2'-ethyl-hexyloxy)(MEH) with HOMO below the fermi level of gold. The bandgap of MEH-PPV is ca. 2.47 eV [14] that is suitable for using as an emission layer in OLEDs or a photoactive layer in OSCs.

2.6. Poly(3-hexylthiophene) (P3HT)

P3HT is a type of conducting polymer that is used for flexible polymer electronic devices like organic solar cells and gas sensors. P3HT with an energy bandgap of 1.9 eV [19] is often used as the electron donor in a bulk heterojunction. The molecular structure of is shown in Fig. 8.

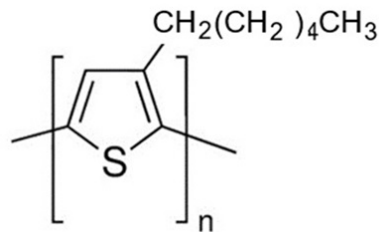


Fig. 8. Molecular structure of P3HT [19].

3. Some optoelectronic devices made from nanocomposites

In this section we analyze main results of the overseas researches, included of ourselves on nanocomposite materials used for optoelectronic devices. Similar to inorganic semiconducting materials, conducting polymers possess an energy band structure with a bandgap, separating between the HOMO and LUMO levels (for inorganic semiconductors there are the valence and conducting bands). When applying an external electric field, after the formation of EHPs (namely, *excitons*) and in case EHPs are not recombined, electrons and holes move to the opposite directions, as shown in Fig. 9.

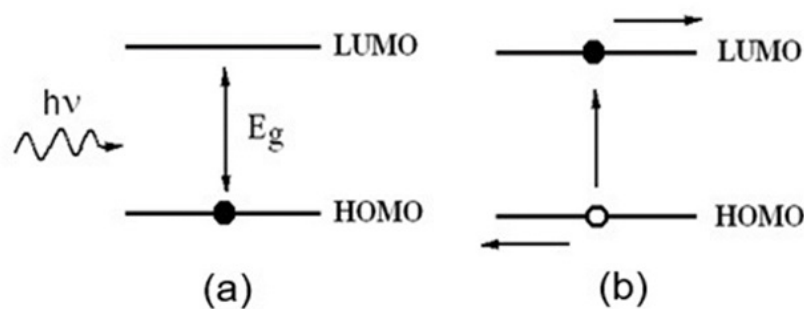


Fig. 9. Formation of excitons (a) and the excitons dissociation (b) [20].

Regarding to polymeric nanocomposites, the main differences from CPs are the heterojunctions formed in the composites which strongly affect the excitons decay process. Polymeric nanocomposites are easy prepared by embedding nanoparticles/nanocrystals or QDs in pristine CPs. The enhancement of both the efficiency and service duration of the nanocomposite devices can be reached by adding inorganic nanostructured additives particles. The next section gives an overview analysis of the influence of nanoparticles on the characteristic properties of three types of optoelectronic devices, namely OLEDs, OSCs and OGSs.

3.1. Organic light-emitting diodes (OLEDs)

OLEDs have many advantages over inorganic LEDs, such as easy fabrication process, large-area emission, possible flexible devices, etc. However, there are considerable limitations of OLEDs for instance, fast aging of both the materials and devices, low performance efficiency, etc. In difference from LEDs, OLEDs consist of thin-film layers where the first layer is a transparent conducting electrode (TCE) that is often deposited onto glass substrates or flexible polymethyl methacrylate (PMMA). Due to a high work function, Sn-doped In_2O_3 (ITO) is preferred to used for the transparent anode. Next to the TCE, there is a hole transport layer (HTL), then an emission layer (EML), an electron transport layer (ETL), and a metallic cathode (Fig. 10). The metallic cathode (Al or Mg) is a mirror-like layer, reflecting light emitted from EML, consequently contributes to the enhanced lighting efficiency of devices.

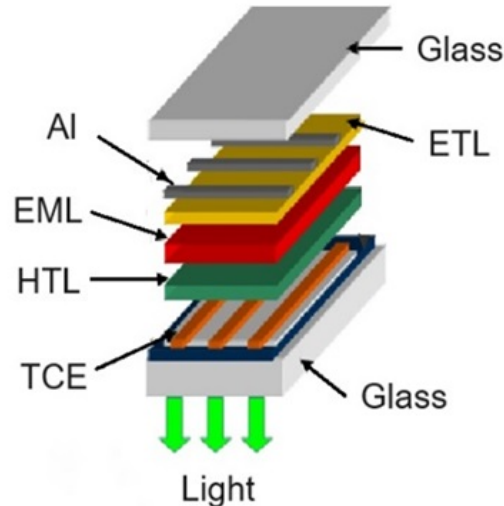


Fig. 10. Structure a laminar OLED.

Each polymeric thin layer (namely EML, HTL and ETL) is the specific conducting one. Recently, to enhance both the performance efficiency and the lifetime of devices, these layers were replaced by their composites with inorganic nanoparticles of ZnO (ns-ZnO), TiO_2 (nc- TiO_2), nano-semiconductors, QDs or carbon-based nanomaterials (CNT, rGO, G) etc. [21, 22].

As reported in [23], Nguyen et al. have prepared nanocomposite films of PEDOT-PSS and nc- TiO_2 for the HTL in OLEDs. This because PEDOT-PSS possesses a high transmission and a large conductivity [24, 25]. Homogenous distribution of nc- TiO_2 particles in PEDOT-PSS was observed by AFM micrographs (Fig. 11).

For OLEDs made from all the nanocomposite component layers (namely HTL, EML and ETL), Nguyen et al. [23] have demonstrated that the current-voltage (I - V) curve was much enhanced in comparison with that of the other devices (Fig. 12). The efficiency of these OLEDs increased about 35%, whereas the thermal stability was also improved. This is explained due to

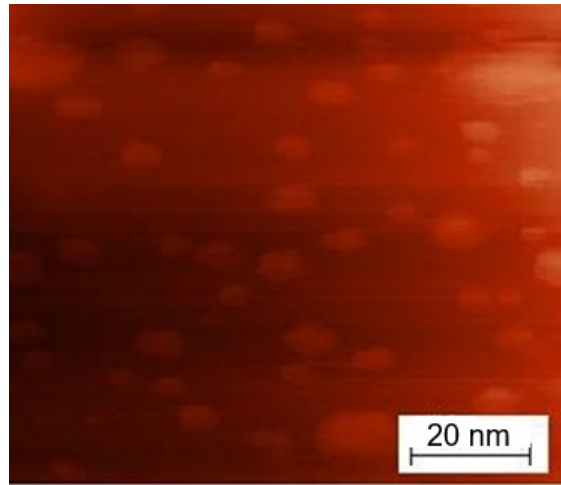


Fig. 11. AFM of the nanocomposite PEDOT-PSS+TiO₂ film used for HTL in OLED. 20 wt.% nc-TiO₂ was embedded in polymer [23].

numerous nc-TiO₂/polymer heterojunctions created in nanocomposite layers, and due to eliminating the thermal power generated from Joule-Lenz current.

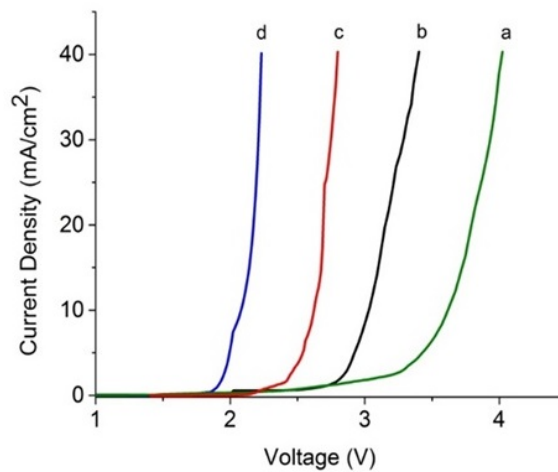


Fig. 12. *I-V* characteristics of OLEDs with (a) Single pristine EML (MEH-PPV), (b) Standard HTL (PEDOT-PSS), (c) Composite HTL and EML, and (d) all composites [23].

In a work of Al-Asbahi [26], poly(9,9-di-n-octylfluorenyl-2,7-diyl) (PFO) was used as an additive in the composite EML. The authors used both planar (SiO₂/TiO₂+MEH-PPV) and bulk SiO₂/TiO₂+PFO/MEH-PPV heterojunctions for EML. Comparing Fig. 13 (a) and Fig. 13 (b) one can see that with the addition of SiO₂/TiO₂ in PFO/MEH-PPV, the *I-V* curves were improved considerably: the current density increased more than 40-times, whereas the turn-on voltage decreased around three times. Moreover, in case of nanocomposite OLEDs at the turn-on voltage,

the current quickly increased. This demonstrates that the charges (electrons and holes) balance has been obtained in the EML of the OLEDs, resulting in the increase of the emission efficiency of the composite OLEDs, namely about 30% in comparison with standard polymer devices [26].

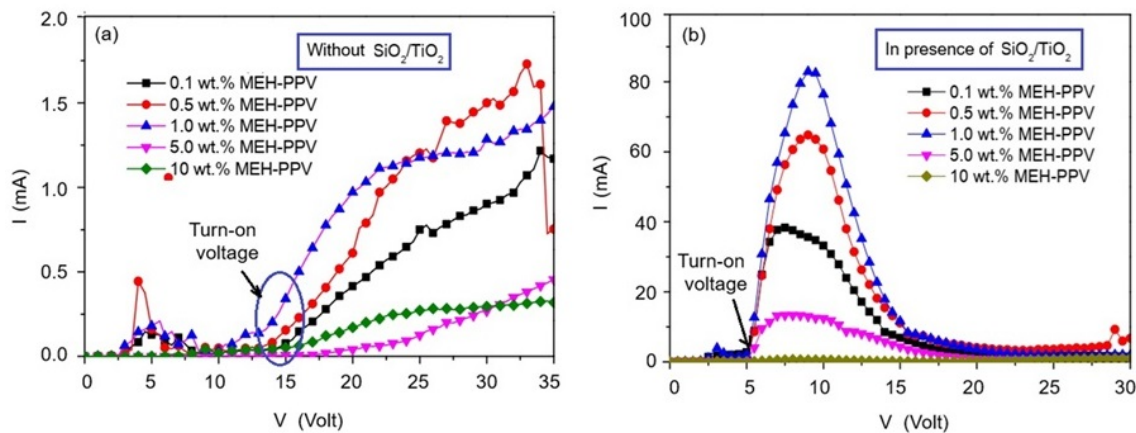


Fig. 13. *I-V* characteristics of OLED based on PFO/MEH-PPV without (a) and with of $\text{SiO}_2/\text{TiO}_2$ (b) The optimal percentage of the MEH-PPV in PFO is 1 wt.% [26].

Bis(3-(3,5-bis(dodecyloxy)phenyl)-(5-pyridin-2-yl)pyrazolate)platinum(II) complex (PT12) was used as a dopant in PFO [27]. The color coordinates of the devices exhibited a broad shift in the CIE color space. Interestingly, Cuerva et al. showed that with a suitable addition of PT12, white-OLEDs for solid-state lighting (SSL) can be produced [28].

QDs made by CdSe/ZnS combined with poly[(9,9-di-n-octylfluorenyl-2,7-diyl)-alt-(benzo[2,1,3]thiadiazol-4,8-diyl)] (F8BT) were used for the EML in OLEDs [29]. The authors made bulk heterojunctions in the composites by mixing QDs with F8BT, whereas planar heterojunctions were made by coating QDs onto F8BT. These composite films emitted a broad peak of 500 - 700 nm that has been attributed due to the contribution of the emission of 540 nm from the polymer and the emission of 634 nm from QDs. For planar structures, QDs substantially contributed to the fluorescence spectrum. As reported in [29], OLEDs with the EML of 15 wt.% QDs embedded in polymers have the largest luminance efficiency, the turn-on voltage is slightly larger comparing to pristine polymer devices. Polythiophene/ SnO_2 nanocomposites (PTh- SnO_2) have been synthesized for EML in OLEDs, this EML emitted blue-green colour, near to white light [30]. The authors explained this due to the addition of nc- SnO_2 in PTh- SnO_2 nanocomposites, resulting in lowering optical band gap of the material down to 2.07 eV. It was shown that the thermal stability of samples with 15% PTh- SnO_2 is much better in comparison with the pure polythiophene.

As reported in [31], Metal-Organic Frameworks (MOFs) were also used as the additive in EMLs for OLEDs, since MOFs exhibited a good fluorescence lifetime, a large quantum efficiency and an excellent tunability. With the addition of MOFs in EMLs, both the Correlated Color Temperature (CCT) and Color Rendering Index(CRI) values of OLEDs were much improved, resulting in widening the color emission spectrum range. This suggests potential applications of the

MOFs in OLED industry. In a recent work [32], a composite of PEDOT:PSS and graphene oxide (PEDOT:PSS-GO) was used for the HTL in perovskite light-emitting diodes (PeLEDs), where perovskite $\text{CH}_3\text{NH}_3\text{PbBr}_3$ was used for the EML. The work function of PEDOT:PSS-GO HTL has been increased, whereas the hole injection barrier at the HTL/EML interface was decreased. This proves that GO additive in PEDOT:PSS resulted in reducing the luminescence quenching from the emission layer. Fig. 14 (a) shows the current dependence of the luminance of the PeLED.

For PeLEDs using pure PEDOT:PSS as the HTL, the maximum luminance intensity is of ca. $2,305 \text{ cd/m}^2$, whereas the devices with PEDOT:PSS-GO served as the HTL have the value of the maximum luminance intensity as large as $3,302 \text{ cd.m}^2$ (43.3% larger in comparison with the value of the undoped device). Fig. 14 (b) shows the voltage dependence of current density for the PeLEDs with the HTLs doped by different GO contents. The turn-on voltage is lowered from 4.30 V to 3.87 V with the increase of GO ratio from 0 to 0.5. The authors explained this effect due to the efficient hole injection, but the GO ratio larger 0.5 resulted in opposite effect, i.e. the efficiency for the device fast decreased.

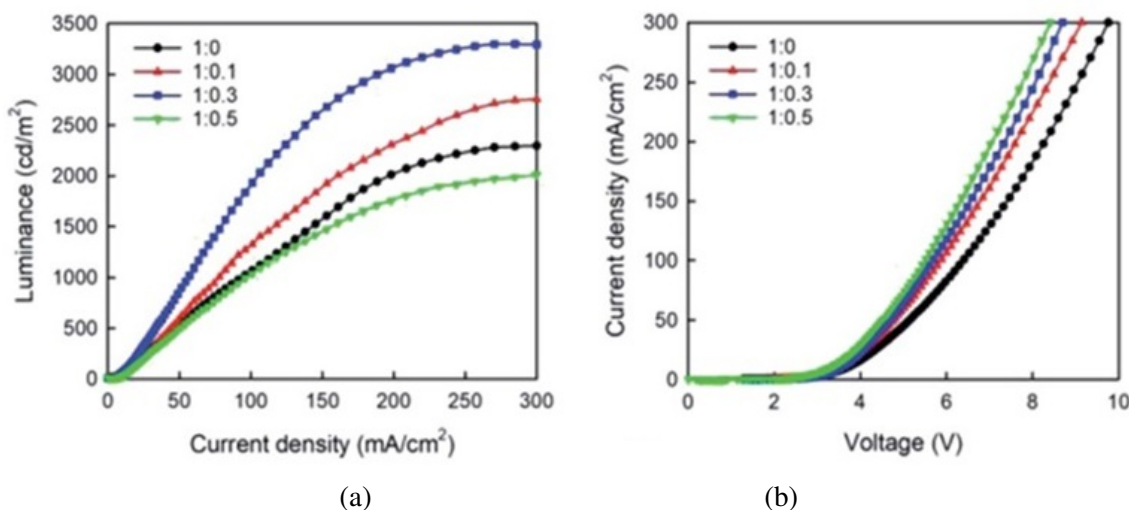


Fig. 14. Performance characteristics of PeLEDs: (a) Luminance vs. current density, (b) Current density vs. voltage [32].

By embedding nc-MoS₂ in PEDOT:PSS, nanocomposite HTL with a MoS₂/PEDOT:PSS ratio of 3.3%, 6.6%, and 10% have been made [33]. By using spin-coating, 30 nm-thick composite HTL films were deposited onto ITO substrates. At $\lambda = 450 \text{ nm}$, the HTL films have a transparency of ca. 90%, showing that nc-MoS₂ nanoparticles not much affected the transparency of PEDOT:PSS. The authors of [33] demonstrated that nc-MoS₂ nanoparticles enabled to prolong the lifetime of the devices under standard ambient up to 1,000 hours. The work function of the HTL has also been enhanced due to the addition of MoS₂ in polymers. A recent review work [34] showed that different types of nanoparticles like metallic-based, carbon-based, organic, inorganic, and hybrid nanoparticles which were embedded in PEDOT:PSS used for the HTL considerably affected the performance parameters of OLEDs. Herein, the authors pointed out that the surface

plasmon resonance (SPR) from metallic-based nanoparticles facilitated charge transport and electrical properties of PEDOT:PSS.

Core-shell nanoparticles were embedded in PEDOT:PSS polymer for the modification of HTL [35]. These core-shell nanoparticles were prepared by covering silver nanoparticles (Ag-NPs) with W-polyoxometalate compound (POM/Ag-NPs). The authors demonstrated that Ag-NPs generated the plasmonic phenomenon in the HTL helping the balance of the hole and electron movements to the EML. Thus, the performance efficiency of the devices is enhanced. The effect of the POM/Ag-NPs on the enhancement of the efficiency of OLEDs was studied by combining electrical measurements with the UV-Vis spectra, AFM micrographs, and photoluminescence (Fig. 15). The obtained results showed that the hole-electron charge balance and exciton recombination rate have been enhanced. In [35] POM gold NPs (POM/Au-NPs) were also added into the polymers for the comparison between two metallic nanoparticles (namely Au-NPs and Ag-NPs). As a result, the POM-Ag NPs exhibited considerable advantages over the POM/Au-NPs. The authors showed that the approach using core-shell nanoparticles in polymers has considerably contributed to the production of the high-quality composite OLEDs.

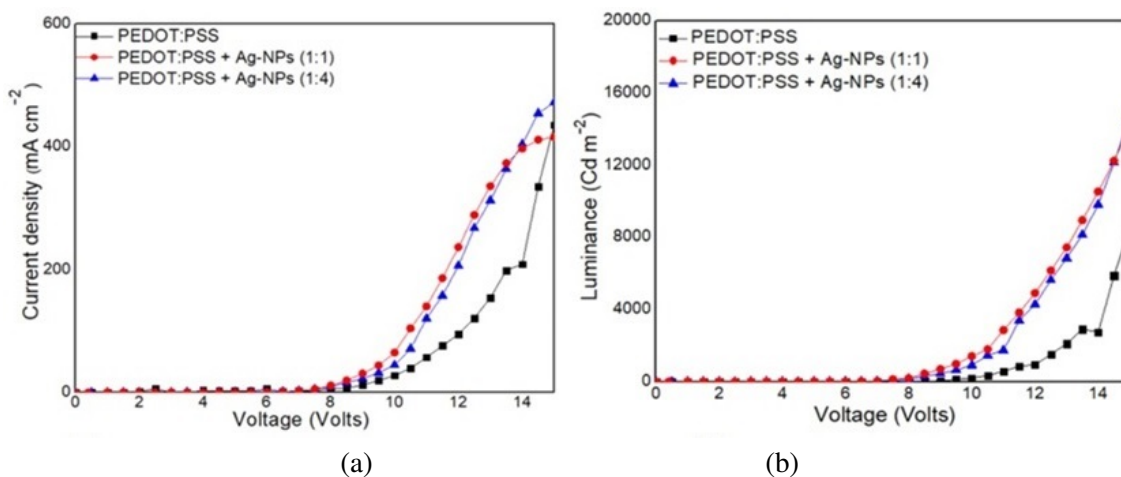


Fig. 15. Ag-NPs concentration effect of the POM/Ag-NPs embedded in HTL: I-V characteristics (a) and Electro-Luminance of the OLED vs voltages (b) [35].

3.2. Organic solar cells (OSCs)

Comparing with inorganic (c-Si) solar cells, OSCs have many advantages such as simple-technology processes, possible large-area panels, easy installations, etc. However, OSCs have also disadvantages, such as low performance efficiency, fast aging, impossible working at high humidity and temperatures. There are several ways to overcome above-mentioned disadvantages, one of them is to make polymeric nanocomposite used in devices. Distinguishing Si-solar cells where there are p-n junctions, OSCs consist of heterojunctions of different organic semiconducting materials. OSCs usually have five layers: a positive electrode (e.g. ITO-coated substrate), a hole transport layer (HTL), a photoactive layer (PhL), an electron transport layer (ETL), and a negative electrode acting as a large reflector (e.g. Al) (Fig. 16). The PhL layer often consists of

donor/acceptor heterojunctions. As shown in [36], highly-efficient devices were prepared by using bulk heterojunctions of fullerene derivatives (donors) and polymers (acceptors). The operation steps of these OSCs occurred as follows. Under solar exposing, electrons generated in the donor layer jumped to acceptor layer, forming the EHPs (excitons). At the moment, a local electrical field occurred in the PhL resulting in the charge separation. Due to the HTL and ETL, electrons moved to the negative electrode and holes - to the positive one, creating so-called open-circuit voltage (V_{oc}). If the circuit is short, a short-circuit current can be obtained. In almost measurements a short-current density that is the current per area unit (J_{sc}) is used instead of the short-circuit current.

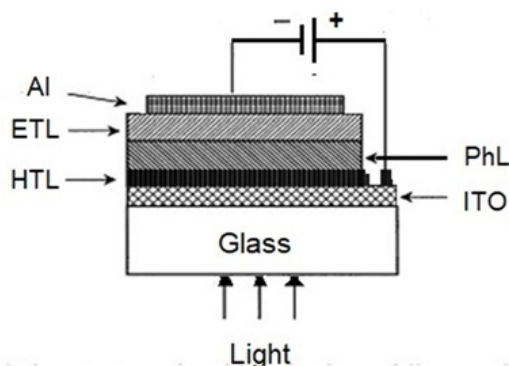


Fig. 16. Schematic drawing of a laminar organic solar cell.

To enhance the thermal endurance of OSCs, Tran et al. [37] have prepared nanocomposite PhL film by embedding nc-TiO₂ in P3HT polymer (P3HT+nc-TiO₂). This is based on the better thermal endurance and stability of the composite film [38] where the authors demonstrated that the thermal expansion coefficient (α) of the P3HT+nc-TiO₂ composite PhL is much smaller than the one of the pristine P3HT. The enhanced performance parameters of the composite-based OSCs operating at elevated temperatures have been demonstrated by the comparison of two devices: the first one was prepared from a pristine P3HT-PhL and the second one was made from a nanocomposite PhL, namely ([6,6]-phenyl C61 butyric acid methylester (PCBM)/P3HT mixed with nc-TiO₂). The thermal expansion properties of both PhL materials and P-V devices have been studied on AFM images and I-V characteristics, respectively. Herein, the annealing effect on the morphology of the pristine polymer and nanocomposite PhL was clearly observed (see Fig. 17): for the pristine P3HT annealed at 130 °C, many large pores occurred, whereas for the composite PhL annealed at the same temperature, nc-TiO₂ particles were filled-up the pores. Consequently, the pores acting as the charge traps in the PhL have been eliminated, resulting in the increase of the FF, V_{oc} , and J_{sc} . It is known that the photoelectrical conversion efficiency (PCE) of OSCs is determined by $PCE = (FF \times V_{oc} \times J_{sc}) / P_{in}$ (where P_{in} is the density of the illuminating power), thus PCE of the composite device increased due to with the increase of FF and V_{oc} , J_{sc} .

As shown in [37], at 60 °C, the maximum value of the PCE of the OSC using pristine P3HT as the PhL reached only 1.6%, and fast decreased to zero at 140 °C (Fig. 18). Whereas, the

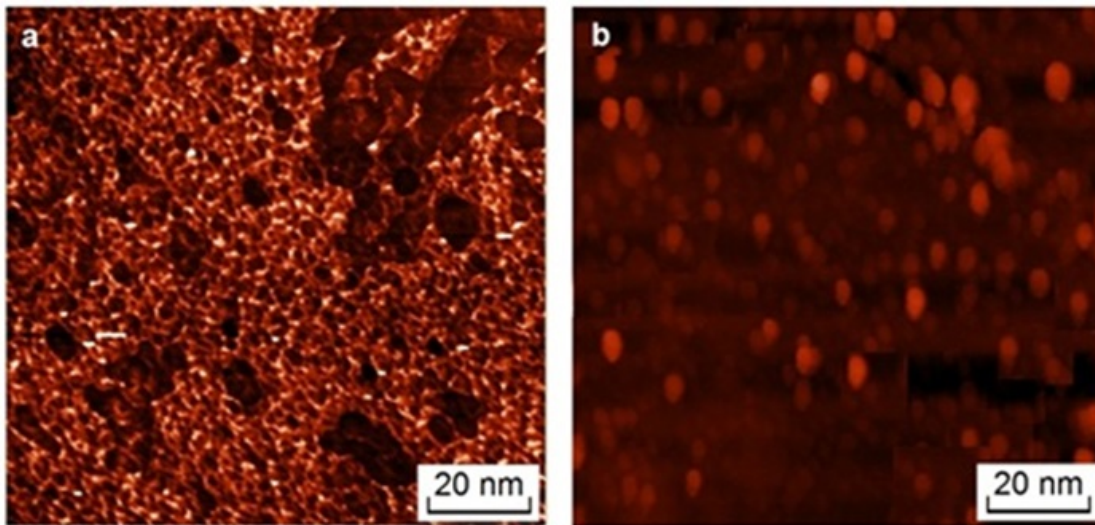


Fig. 17. The annealing effect on the morphology of the photoactive layers in OSCs: AFM micrograph of pristine P3HT (a) and composite P3HT (5 wt.% nc-TiO₂) (b) [37].

composite devices still worked and their PCE lowered to a value of 1.2%. The authors explained this due to the improved thermal expansion coefficient of the composite PhL material, $\alpha = 0.91 \times 10^{-5} \text{ K}^{-1}$ that is much smaller than the one of the pristine PhL ($\alpha = 7.60 \times 10^{-5} \text{ K}^{-1}$) [38]. In the polymer, with increasing temperature, the pores appeared and fast expanded, generating large defects which trapped both holes and electrons. For the composite PhL, in the nc-TiO₂/P3HT interfaces there are numerous heterojunctions replacing pores, and the charge carriers easy moved through the interfaces and faster reached the electrodes. Thus, the fill factor (FF) of the devices increased, consequently both the V_{oc} and J_{sc} also increased. As a result, the PCE of the OSCs with PhL is much larger than the one of the devices using the pristine polymer PhL material (Fig. 18). From this figure one can see that at 70°C the PCE of the composite devices has a value as large as 2.2%. This means that the effective temperature range for the composite solar cell is from 60–80 °C that is lower than the effective temperature range for some types of inorganic solar cells [39].

Metal-oxide nanoparticles (MNPs) were also used for preparing both OSCs and perovskite solar cells (PSCs) [40]. Nanoparticles of ZnO, TiO₂ were used as the electron-transport materials [41, 42], while NiO_xNPs, Cu-doped NiO_xNPs, and graphene oxide (GO) functionalized with MoO_xNPs were used as hole-transport materials [43, 44]. It is shown that embedding MNPs in polymeric layers has efficiently improved the thermal stability of both the OSCs and PSCs, especially when the polymers are coated on top of the active layers. Metal-oxide nanorods (MNRs) embedded in the active layers of OSCs were also investigated [45, 46]. With use of the combination of ZnO-NRs and TiO₂-NRs, the authors proved the enhancement of the charge separation efficiency. As reported in [47], Nguyen et al. have shown a supper thin ZnO layer deposited onto ITO electrode has acted as a buffer layer between the ITO electrode and the hole transport layer. By this way, the FF of the OSCs much increased, resulting in the increase of the PCE nearly 30%.

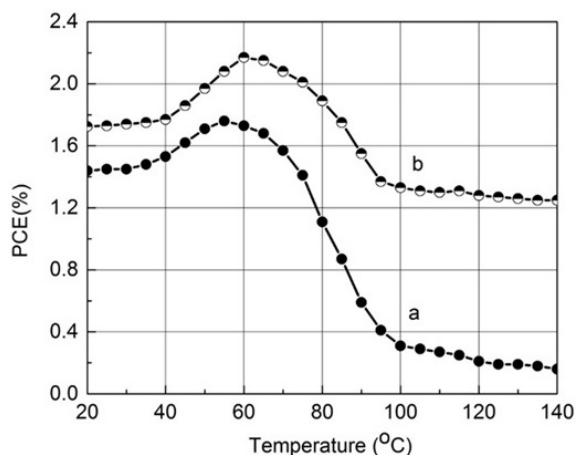


Fig. 18. The influence of working temperature on the PCEs for the OSCs with a pristine PhL material (curve “a”) and for the OSCs with a composite PhL (curve “b”) [37].

Indeed, it has increased from PCE = 1.75% (for OSCs without ZnO) to 2.12% (for OSCs with ZnO).

As reported in [48] the MNPs caused the localized surface plasmonic resonance (LSPR). This also affected to the performance parameters, especially the PCE of OSCs. With the presence of the LSPR, the exciton dissociation has been strongly enhanced, resulting in the charge carrier's separation and elimination of the hole-electron recombination. Besides, the LSPR effect of MNPs contributed in the enhancement of the electromagnetic field, activating a strong photoabsorption and generation of excitons in the PhL materials. Due to the light scattering in PhL materials, the effect of the exciton generation increased [49]. Moreover, generated excitons combined with the MNPs in the electromagnetic field also facilitated the charge separation, resulting in improving the performance parameters (FF, V_{oc} and J_{sc}) of the composite OSCs. Although the MNPs can be embedded in all functional layers of the bulk-heterojunctions (BHJ) OSCs [50], it is more efficient if they are added in the PhL, since the LSPR effect may disappear over few nanometers [51]. As reported in [52], by using a graphene additive in pristine P3HT (G-P3HT) served as the PhL, one can enhance both the optical and spectral properties of P3HT. In the G-content range of 0.1 - 5.0 wt.%, the additive with 1.0 wt.% G was found to be optimum for the OSCs performance. This enhancement was explained due to both the lowering of the bandgap and better hole collection efficiency, carrier mobility, refractive index, and the extinction coefficient.

In [53] ZnO nanoparticles were embedded in pristine PANI (PANI-ZnO) used as the donor material in composite OSCs. The composite devices with a laminar structure of ITO/P3HT/PANI-ZnO/Ag (abbreviated to PPZ) were made by a spin-coating technique. I-V curves of the PPZs devices were measured under illuminating by AM 1.5G with a power density of 100 mW/cm² as shown in Fig. 19. It is clearly seen that the current (or J_{sc}) of the cells are strongly dependent on the concentration of ZnO nanoparticles (ZnO NPs) embedded in PANI. The obtained results have demonstrated that the optimum concentration of ZnO NPs is of 3.0 wt.%. According to this optimum ZnO NPs concentration, the PCE of the composite PPZs devices was found to be of 4.48

% that is much larger than the one of the devices using pristine PANI, namely only 3.10 % as reported in [53].

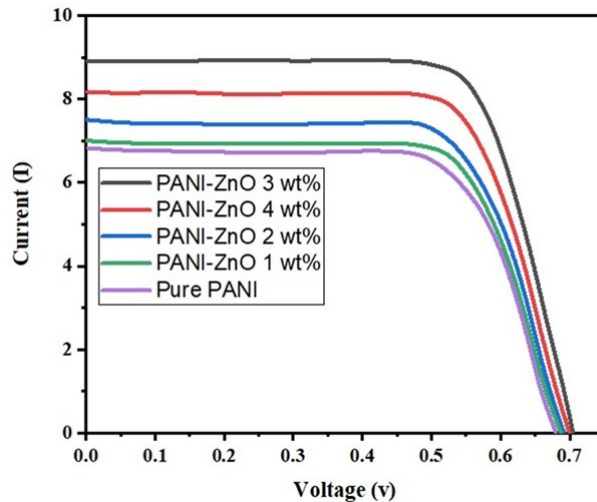


Fig. 19. I-V characteristics of ITO/P3HT/PANI-ZnO/Ag with use of a pristine PANI (the lowest curve) and ZnO NPs/PANI (1, 2, 3, and 4 wt.% of ZnO NPs) as the donor materials in the devices [53].

Using MNPs for the interface modification of the HTL in OSCs has resulted in the charge separation. Moreover, a better ohmic contact between HTL and electrodes in composite devices has also been enhanced [54]. A mixture of Fe_3O_4 and GO ($\text{Fe}_3\text{O}_4/\text{GO}$) nanocomposite was used as the secondary additive in PEDOT:PSS to make OSCs with a large performance efficiency. This composite HTL has not only a high transmittance, but also a large value of the work function. The authors of [54] indicated that as $\text{Fe}_3\text{O}_4/\text{GO}$ is a magnetic compound, when doping it in PEDOT:PSS, one can get an improved conductivity of the HTL. Doping with an optimum concentration of $\text{Fe}_3\text{O}_4/\text{GO}$, the PCE of the composite OSCs measured in experiments has been found to be of 18.91%.

3.3. Organic film gas sensors (OGSs)

Distinguishing from OLEDs and OSCs, organic thin film gas sensors (OGSs) possess a considerably simple structure which may consist of a single layer of a pristine polymer or a composite material and two separated Pt electrodes (Fig. 20). Nanocomposite sensors can be made by mixing pristine polymers (namely PEDOT:PSS, P3HT, and PFO, etc.) and inorganic additives such as nc- TiO_2 , nc-ZnO, CNTs, and graphene quantum dots (GQDs). The working principle of the resistance sensors is as follows, a gas absorbed on the sensor's surface results in the change of the sensor resistance vs the gas concentration in ambience. A sensitive sensor can detect gases with a concentration of few ppm [55].

In [56] Olenych et al. have made sensors based on PEDOT:PSS doped with porous silicon (PS) and CNTs (PEDOT:PSS-PS-CNTs) for detecting gases in atmospheric ambience. The authors indicated that for PEDOT:PSS-PS-CNTs composite films, the considerable influence of

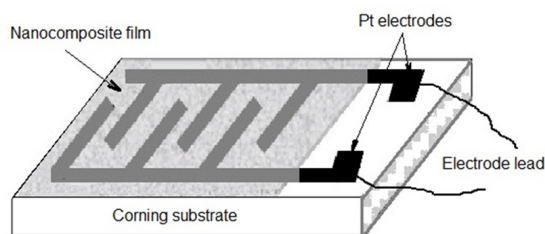


Fig. 20. Schematic drawing of a thin film gas sensor.

atmospheric conditions like humidity, temperature to both the electrical resistance and capacitance of the composite films. The dynamic dependencies for the PEDOT:PSS-PS-CNTs composite sensor were characterized by $R-t$ and $C-t$ curves. These effects were explained due to the increase of electrical conductivity of the sensors during the composite surface contacting with H_2O molecules [57].

As reported in [58], to avoid uncontrolled effects of the modification of the commercial CNTs surface before embedding in polymers, the authors used directly pitch to make so-called carbon replica (CR). Using nano-casting method reported in [59], CRs were made by replacing nc- SiO_2 templates of 10 nm in size due to HF acid etching. Then CR-P3HT (P3C) solution with a weight ratio 0.10 of CR/polymer was deposited by spin-coating on the grid ITO electrodes to get P3C sensors. P3C composite sensors were exposed to NH_3 gas with a concentration C_{gas} of 10, 20, 30, 40 and 50 ppm. The obtained results of detecting NH_3 vs. exposing (adsorption) and out (desorption) time are shown in Fig. 21. It is seen that the response time of P3C sensors is of 30 s, the sensing response obtained at the NH_3 concentration decreasing from 50 to 40, 30, 20, and 10 ppm was found to be of 6.78, 5.27, 3.75, 2.72, and 1.97, respectively (Fig. 21).

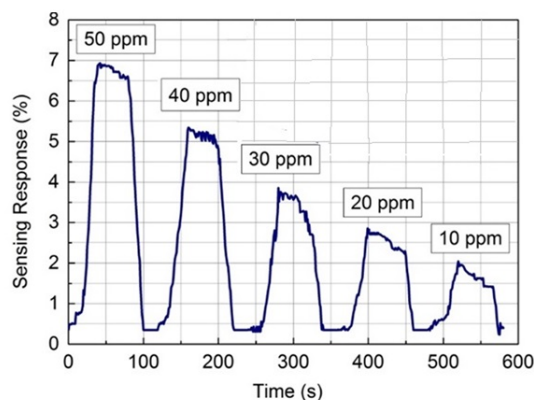


Fig. 21. NH_3 gas monitoring of composite P3C sensors [58].

Thus, with the addition of CRs in pristine P3HT, an enhanced sensitivity of the composite sensors was obtained. Similar to the other composites, CRs-P3HT films possess numerous heterojunctions formed between the P3HT and carbon nanospheres, resulting in faster charge transferring

and improvement of the adsorption efficiency of NH_3 molecules. This efficiently contributed in the enhancement of the sensing response of such resistive sensors as composite CRs-P3HT.

OGSs have also been prepared by a simple drop-casting method where a grid ITO-coated glass was used as the substrate [60]. A mixture composite made from pristine P3HT, reduced graphene oxides (rGO) and carbon nanotubes (CNTs) (abbreviated to PGCs) was used as the sensitive layer to NH_3 gas. The PGS solutions were dropped onto the grid ITO substrates, then annealed for drying getting solid PGS sensors. The resistances between two ends of the electrodes for the initial PGSs and for PGSs exposed in NH_3 was measured using a 2400-Keithley power meter. The results obtained in experiments measuring the sensors resistances vs. the weight ratio of the three components showed that the sensor with the ratio of 20%:60%:20%, respectively to P3HT:rGO:CNTs was the best for detecting NH_3 . The performance parameters of this sensor (abbreviated to PGC-60) were found to be of 30 s (response time) and 3.6% (sensitivity) at NH_3 concentration of 10 ppm; and a relative sensitivity of 0.031%/ppm was reached. The authors of [60] explained the enhancement of the sensitivity of P3HT:rGO:CNTs composite sensors due to the efficient NH_3 adsorption of P3HT, improvement of the electron transport of rGO, and fast movement of holes from the polymer to cathodes due to the CNT nano-bridges. An optimum P3HT/rGO/CNTs ratio for detecting NH_3 gas was found to be of 20/60/20 (namely, sensor PGC-60, curve "b" in Fig. 22). Recent work [61] showed that the nanocomposites have been efficiently used for different applications included gases sensors, bio-sensors, and chemical sensors. The enhanced parameters of sensors like sensitivity, selectivity and response time can be obtained by choosing appropriate nanocomposites to attain the efficient interactions between the molecules of gases and the nanocomposite surfaces. From the interactions one can define the sensing mechanism of the composite devices. The authors of [61] used composites of a mixture of molecularly imprinted polymer (MIP), PANI and copper oxide nanoparticles (CuONPs) for monitoring blood glucose levels (BGL) in humans. To modify graphite electrode, CuONPs were coated onto the bare graphite by electrochemical deposition in H_2SO_4 solution. With use of the modified G-electrodes, the selectivity of the glucose sensors was considerably improved.

PANI/ZnO-NPs nanocomposites used for NH_3 sensors have made by covering ZnO-NPs with PANI [62]. Li et al. showed that the form of the nanocomposites considerably affects the sensing response of the devices. The PANI/ZnO composite with ZnO nanorods (PANI/ZnO-NRs) has a very low detection limit (Fig. 23a) significant change in the resistance when exposed to NH_3 concentrations as low as 5 ppm, exceptional repeatability, and excellent selectivity (Fig. 23b).

The authors of [63–65] used composites of PANI/G or PANI/G-based forms for making gas sensors, ion sensors, and bio-sensors. Wu et al. [66] used the Ppy, PANI, and G-nanofiller nanocomposite for different kinds of sensors. These nanocomposite-based sensors were also used to monitoring the volatile sulfur compounds and NH_3 gases. The useful informations of the development in gas sensors based on the polymeric nanocomposites are given in [67, 68]. The authors revealed the role of inorganic nanomaterials including metal oxides, metal, carbon (CNT, G and rGO) in the enhancement of the performance parameters of gas polymeric sensors.

There are many other gases like NO_2 , H_2S , LPG, H_2 , etc. in ambience have also been monitored using appropriate nanocomposite-based sensors. Since the limitation of an article length, this section is concerned to some polymeric nanocomposites used for gas sensors. More detailed discussions on the sensing properties of different nanocomposite-based sensors are referred in a recent review [69].

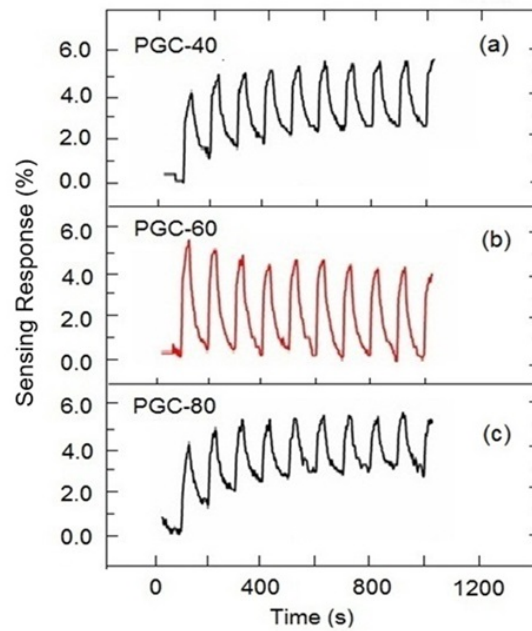


Fig. 22. Sensitivity vs. rGO concentration embedded in P3HT:rGO:CNTs composites with a weight ratio of P3HT/rGO/CNTs equal to 30/40/30, 20/60/20, and 10/80/10, as shown respectively in (a), (b) and (c). The measurements of the resistances were carried-out at 10 ppm of NH_3 concentration [60].

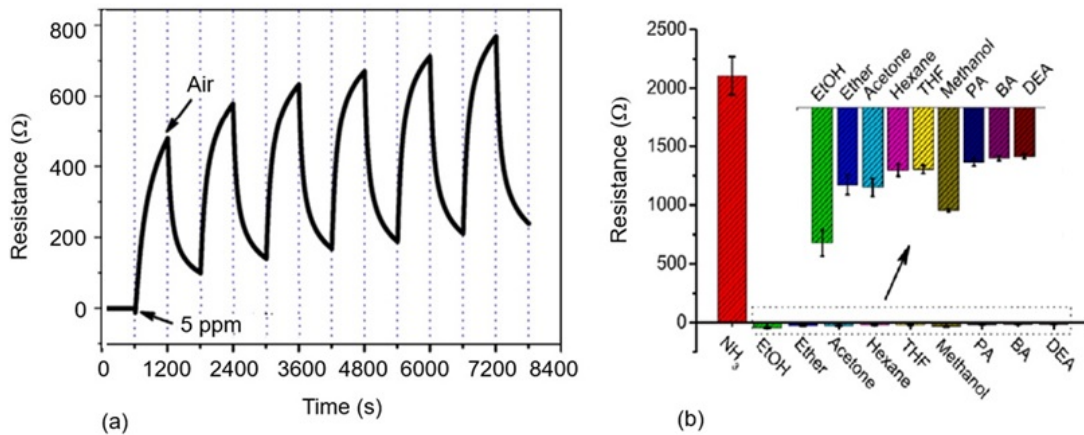


Fig. 23. Sensing response (a) and Selectivity (b) of PANI/ZnO-NRs composite towards NH_3 gas [62].

4. Conclusions

In summary, in this work a topical review is given on the electrically conducting polymers and polymeric nanocomposites. With embedding nanostructured additives of MNPs, CNTs, QDs,

rGO etc. in conducting polymers, all their properties like the thermal, mechanical, and physical have been considerably improved. This is explained due to (i) the elimination of nanopores (acting as the charge carriers traps in CPs), and (ii) the formation of numerous heterojunctions in the nanocomposites. These advantages of the nanocomposite materials suggest prospective applications of the nanocomposites in further organic optoelectronics.

For more efficient applications of the nanocomposites, future investigations should be concentrated to deal with following topical areas:

- (1) Environmentally friendly technologies that can reduce both the energy consumption and carbon footprint.
- (2) Artificial intelligence (AI) exploitation to design and optimize nanostructured polymeric composites for the efficient use of resources and faster developing materials applications.
- (3) 3D printing technology to enhance manufacturing polymeric nanocomposites with the precise control of their structure and properties.

Combining these advancements, one can find out principal solutions for a wide range of efficient applications of polymeric nanocomposites.

Conflict of interest

The author declares that there are no competing interests related to this article.

References

- [1] J. S. Salafsky, *Exciton dissociation, charge transport, and recombination in ultrathin, conjugated polymer, TiO₂ nanocrystal intermixed composites*, *Phys. Rev. B* **59** (1999) 10885.
- [2] W. U. Huynh, J. J. Dittmer and A. P. Alivisatos, *Hybrid nanorod, polymer solar cells*, *Science* **295** (2002) 2425.
- [3] T. M. Petrella, M. Tamborra, A. Agostiano, M. Striccoli, G. L. Guerriero, A. Cola *et al.*, *TiO₂ nanocrystals – MEH-PPV composite thin films as photoactive material*, *Thin Solid Films* **451-452** (2004) 64.
- [4] V. M. Burlakov, K. Kawata, H. E. Assender, G. A. D. Briggs, A. Ruseckas and I. D. W. Samuel, *Discrete hopping model of exciton transport in disordered media*, *Phys. Rev. B* **72** (2005) 075206.
- [5] M. Zhang, S. Höfle, J. Czolk, A. Mertens and A. Colmann, *All-solution processed transparent organic light emitting diodes*, *Nanoscale* **7** (2015) 20009.
- [6] I. A. Rashid, M. A. Al-Maadeed, M. A. Wahab, M. A. Al-Maadeed, M. A. Wahab and M. A. Al-Maadeed, *Electrically conductive epoxy/polyaniline composite fabrication and characterization for electronic applications*, *J. Reinf. Plast. Compos.* **41** (2021) 34.
- [7] E. Carlos, R. Martins, E. Fortunato and R. Branquinho, *Solution combustion synthesis: towards a sustainable approach for metal oxides*, *Chem. Eur. J.* **26** (2020) 375.
- [8] D. Bokov, A. Jalil, M. Chupradit, M. S. Ansari, M. K. Amini and M. K. Amini, *Nanomaterial by sol-gel method: synthesis and application*, *Adv. Mater. Sci. Eng.* **2021** (2021) 5102014.
- [9] Y. H. Jang, S. Hwang, S. B. Chang, J. Ku and D. S. Chung, *Acid dissociation constants of melamine derivatives from density functional theory calculations*, *J. Phys. Chem. A* **113** (2009) 13036.
- [10] A. Elschner, S. Kirchmeyer, W. Lövenich, U. Merker and K. Reuter, *PEDOT: Principles and Applications of an Intrinsically Conductive Polymer*. CRC Press, Taylor & Francis Group, 2011, [10.1201/b10318](https://doi.org/10.1201/b10318).
- [11] H. Letheby, *On the production of a blue substance by the electrolysis of sulphate of aniline*, *J. Chem. Soc.* **15** (1862) 161.
- [12] F. F. Runge, *Poggendorfs ann. phys. u. chemie*, *Poggendorfs Ann. Phys. u. Chemie* **31** (1834) 513.
- [13] G. Schiavon, S. Sitran and G. Zotti, *A simple two-band electrode for in situ conductivity measurements of poly-conjugated conducting polymers*, *Synth. Met.* **32** (1989) 209.

- [14] L. Groenendaal, F. Jonas, D. Freitag, H. Pielartzik and J. R. Reynolds, *Poly(3,4-ethylenedioxythiophene) and its derivatives: Past, present, and future*, *Adv. Mater.* **12** (2000) 481.
- [15] C. K. Chiang, C. R. F. Jr., Y. W. Park, A. J. Heeger, H. Shirakawa, E. J. Louis *et al.*, *Electrical conductivity in doped polyacetylene*, *Phys. Rev. Lett.* **39** (1977) 1098.
- [16] H. Shirakawa, *Die entdeckung der polyacetylenfilme – der beginn des zeitalters leitfähiger polymere*, *Angew. Chem.* **113** (2001) 2642.
- [17] W. J. Feast, J. Tsibouklis, K. L. Pouwer, L. Groenendaal and E. W. Meijer, *Synthesis, processing and material properties of conjugated polymers*, *Polymer* **37** (1996) 5017.
- [18] K. Yamaguchi and T. Tsujioka, *Selective metal-vapor deposition on solvent evaporated polymer surfaces*, *Thin Solid Films* **597** (2015) 220.
- [19] S. Ren, E. K. Stefanakos and D. Y. Goswami, *Inorganic-organic hybrid solar cell: Bridging quantum dot to conjugated polymer nanowires*, *Nano Lett.* **11** (2011) 3998.
- [20] K. J. Klabunde, *Nanoscale Materials in Chemistry*. John Wiley & Sons, 2009.
- [21] V. Mann and V. Rastogi, *Dielectric nanoparticles for the enhancement of oled light extraction efficiency*, *Opt. Commun.* **387** (2017) 202.
- [22] C. Y. Park and B. Choi, *Enhanced light extraction from bottom emission OLEDs by high refractive index nanoparticle scattering layer*, *Nanomaterials* **9** (2019) 1241.
- [23] N. D. Nguyen, H. C. Le, T. C. T. Tran, Q. T. Tran and V. T. Vo, *Enhancement of current-voltage characteristics of multilayer organic light emitting diodes by using nanostructured composite films*, *J. Appl. Phys.* **105** (2009) 093518.
- [24] J. Ouyang, C. W. Chu, F. C. Chen, Q. Xu and Y. Yang, *On the mechanism of conductivity enhancement in poly(3,4-ethylenedioxythiophene):poly(styrene sulfonate) film through solvent treatment*, *Polymer* **45** (2004) 8443.
- [25] P. Tehrani, L. A. A. Pettersson and O. Inganäs, *The effect of ph on the electrochemical over-oxidation in pedot:pss*, *Solid State Ionics* **177** (2007) 3521.
- [26] B. A. Al-Asbahi, *Influence of SiO₂/TiO₂ nanocomposite on the optoelectronic properties of pfo/meh-ppv-based oled devices*, *Polymers* **10** (2018) 800.
- [27] C. Cuerva, J. A. Campo, M. Cano, B. Arredondo, B. Romero, E. Otón *et al.*, *Bis(pyridylpyrazolate)platinum(ii): a mechanochromic complex useful as a dopant for colour-tunable polymer OLEDs*, *New J. Chem.* **39** (2015) 8467.
- [28] M. Belhaj, C. Dridi and H. Elhouichet, *PFE: ZnO hybrid nanocomposites for oled applications: Fabrication and photophysical properties*, *J. Lumin.* **157** (2015) 53.
- [29] C. Borriello, A. Mauro, A. Accardo, M. Barra, A. Cassinese, L. D. Stefano *et al.*, *Optoelectronic properties of OLEDs based on CdSe/ZnS quantum dots and F8BT*, *Phys. Status Solidi C* **12** (2015) 1416.
- [30] R. B. Choudhry and S. Kumar, *Optimum chemical states and localized electronic states of SnO₂ integrated PTh-SnO₂ nanocomposites as excelling emissive layer (EML)*, *Opt. Mater.* **131** (2022) 112736.
- [31] H. Kaur, S. Sundriyal and S. K. Mehta, *Luminescent metal-organic frameworks and their composites: Potential future materials for organic light emitting displays*, *Coord. Chem. Rev.* **401** (2019) 213077.
- [32] Y. Zhou, Y. Wang, Y. Zhang, Y. Wang, Y. Li, Y. Li *et al.*, *Effects of PEDOT:PSS:GO composite hole transport layer on the luminescence of perovskite light-emitting diodes*, *RSC Adv.* **10** (2020) 26381.
- [33] R. Sorrentino, A. Minotto, M. Patrini, M. Meneghetti, F. Meinardi, R. Tubino *et al.*, *Hybrid MoS₂/PEDOT:PSS transporting layers for interface engineering of nanoplatelet-based light-emitting diodes*, *Dalton Trans.* **50** (2021) 9208.
- [34] G. L. Ong, S. S. Lim, S. S. Lim, S. S. Lim, S. S. Lim, S. S. Lim *et al.*, *A brief review of nanoparticles-doped PEDOT:PSS, nanocomposite for oled and opv*, *Nanotechnol. Rev.* **11** (2022) 1870.
- [35] Z. Georgiopoulou, A. K. Andreopoulou, D. Tasis, D. Tasis, D. Tasis, D. Tasis *et al.*, *Plasmonic enhanced oled efficiency upon silver-polyoxometalate core-shell nanoparticle integration into the hole injection/transport layer*, *Sci. Rep.* **14** (2024) 28888.
- [36] I. E. Kuznetsov, A. V. Akkuratov and P. A. Troshin, *Polymer nanocomposites for solar cells: research trends and perspectives*, in *Nanomaterials for Solar Cell Applications*, pp. 557–600, Elsevier, (2019).
- [37] T. T. Tran, Q. T. Tran, V. T. Vo and N. D. Nguyen, *Enhancement of power efficiency and stability of P3HT-based organic solar cells under elevated operating-temperatures by using a nanocomposite photoactive layer*, *J. Nanomater.* (2015) Article ID 463565.

- [38] V. T. Nguyen, V. S. Tran, Q. T. Tran, T. T. Tran and N. D. Nguyen, *Development of laser beam diffraction technique for determination of thermal expansion coefficient of polymeric thin films*, VNU J. Sci. Math. - Phys. **31** (2015) 21.
- [39] D. Meneses-Rodríguez, P. P. Horley, J. González-Hernández, Y. V. Vorobiev and P. N. Gorley, *Photovoltaic solar cells performance at elevated temperatures*, *Sol. Energy* **78** (2005) 243.
- [40] D. Ouyang, Z. Huang and W. C. H. Choy, *Solution-processed metal oxide nanocrystals as carrier transport layers in organic and perovskite solar cells*, *Adv. Funct. Mater.* **29** (2019) 1.
- [41] Z. Zheng, S. Zhang, J. Wang, J. Zhang, D. Zhang, Y. Zhang *et al.*, *Exquisite modulation of ZnO nanoparticle electron transporting layer for high-performance fullerene-free organic solar cell with inverted structure*, *J. Mater. Chem. A* **7** (2019) 3570.
- [42] H. Zhou, Q. Chen, G. Li, S. Luo, T.-B. Song, C. Duan *et al.*, *Interface engineering of highly efficient perovskite solar cells*, *Science* **345** (2014) 542.
- [43] U. Kwon, J. H. Yun, S. H. Lee and S. H. Im, *Solution-processible crystalline NiO nanoparticles for high-performance planar perovskite photovoltaic cells*, *Sci. Rep.* **6** (2016) 30759.
- [44] S. Huang, B. Kang, L. Zhang, L. Liao and D. Zhang, *Enhancing the performance of polymer solar cells using solution-processed copper doped nickel oxide nanoparticles as hole transport layer*, *J. Colloid Interface Sci.* **535** (2019) 308.
- [45] L. Feng and X. T. Hao, *Photophysical behaviors at interfaces between poly(3-hexylthiophene) and zinc oxide nanostructures*, *Mater. Trans.* **58** (2017) 1106.
- [46] X. Li, D. Bi, C. Yi, J. D. Decoppet, J. Luo, S. M. Zakeeruddin *et al.*, *Efficient perovskite solar cells depending on TiO₂ nanorod arrays*, *ACS Appl. Mater. Interfaces* **8** (2016) 21358.
- [47] N. D. Nguyen, H. K. Kim, D. L. Nguyen, D. C. Nguyen and P. H. N. Nguyen, *Characterization of performance parameters of organic solar cells with a buffer ZnO layer*, *Adv. Nat. Sci. Nanosci. Nanotechnol.* **10** (2019) 015005.
- [48] G. T. Mola, A. M. E. Sayed, M. S. Abdel-Wahab, M. M. Rashad and M. M. El-Desoky, *Nanocomposite for solar energy application*, *Nano Hybrids Compos.* **20** (2018) 90.
- [49] J. Liu, S. Li, Y. Li, L. Xu, Y. Wang and Y. Xia, *Recent advances of plasmonic nanoparticles and their applications*, *Materials (Basel)* **11** (2018) 1833.
- [50] R. Ganesamoorthy, G. Sathiyam and P. Sakthivel, *Fullerene based acceptors for efficient bulk heterojunction organic solar cell applications*, *Sol. Energy Mater. Sol. Cells* **161** (2017) 102.
- [51] H. Choi, J.-P. Lee, S.-J. Ko, J.-W. Jung, H. Park, S. Yoo *et al.*, *Multipositional silica-coated silver nanoparticles for high-performance polymer solar cells*, *Nano Lett.* **13** (2013) 2204.
- [52] J. Wang, S. Jia, Y. Cao, W. Wang and P. Yu, *Design principles for nanoparticle plasmon-enhanced organic solar cells*, *Nanoscale Res. Lett.* **13** (2018) 211.
- [53] Alamgeer, M. Tahir, M. R. Sarker, S. Ali, Ibraheem, S. Hussian *et al.*, *Polyaniline/zno hybrid nanocomposite: Morphology, spectroscopy and optimization of zno concentration for photovoltaic applications*, *Polymers* **15** (2023) 363.
- [54] Y. Bao, J. Liu, F. Kerner, N. Schlüter and D. Schröder, *Magnetic nanocomposite modified hybrid hole-transport layer for constructing organic solar cells with high efficiencies*, *ACS Appl. Mater. Interfaces* **16** (2024) 54081.
- [55] T. H. Hoang, T. G. Ho, V. H. Nguyen, T. Tran and V. T. Chu, *Elaboration of pd-nanoparticle decorated polyaniline films for room temperature NH₃ gas sensors*, *Sensors Actuators, B Chem.* **249** (2017) 348.
- [56] I. B. Olenych, O. I. Aksimentyeva, L. S. Monastyrskii, Y. Y. Horbenko and L. I. Yarytska, *Sensory properties of hybrid composites based on poly(3,4-ethylenedioxythiophene)-porous silicon-carbon nanotubes*, *Nanoscale Res. Lett.* **10** (2015) 1.
- [57] I. B. Olenych, L. S. Monastyrskii, O. I. Aksimentyeva and B. S. Sokolovskii, *Humidity sensitive structures on the basis of porous silicon*, *Ukr. J. Phys.* **56** (2011) 1198.
- [58] N. N. Dinh, T. S. T. Khanh, L. M. Long, N. D. Cuong and N. P. H. Nam, *Nanomaterials for organic optoelectronic devices: Organic light-emitting diodes, organics solar cells and organic gas sensors*, *Mater. Trans.* **61** (2020) 1422.
- [59] B. Jache, C. Neumann, J. Becker, B. M. Smarsly and P. Adelhelm, *Towards commercial products by nanocasting: characterization and lithium insertion properties of carbons with a macroporous, interconnected pore structure*, *J. Mater. Chem.* **22** (2012) 10787.

- [60] T. S. T. Khanh, N. D. Hoa, N. V. Duy, N. D. Chien and N. V. Hieu, *Ammonia gas sensing characteristic of P3HT-rGO-MWCNT composite films*, *Appl. Sci.* **11** (2021) 6675.
- [61] S. Jose, S. Das, T. R. Vakamalla and D. Sen, *Electrochemical glucose sensing using molecularly imprinted polyaniline – copper oxide coated electrode*, *Surf. Engin. Appl. Electrochem.* **58** (2022) 260.
- [62] Y. Li, Y. Zhang, X. Zhang, B. Pan, Y. Wang and J. Sun, *High performance gas sensors based on in-situ fabricated ZnO/polyaniline nanocomposite: the effect of morphology on the sensing properties*, *Sens. Actuators B: Chem.* **264** (2018) 285.
- [63] L. Pilan and M. Raicopol, *Highly selective and stable glucose biosensors based on polyaniline/carbon nanotubes composites*, *UPB Sci. Bull. Ser. B* **76** (2014) 155.
- [64] D. Yang, Y. Li, Y. Wang, Y. Zhang, X. Zhang and J. Sun, *Polyaniline-based biological and chemical sensors: Sensing mechanism, configuration design, perspective*, *ACS Appl. Electron. Mater.* **5** (2023) 593.
- [65] D. Aycan, F. Karaca and N. Alemdar, *Development of hyaluronic acid-based electroconductive hydrogel as a sensitive non-enzymatic glucose sensor*, *Mater. Today Commun.* **35** (2023) 105745.
- [66] G. Wu, H. Du, D. Lee, Y. L. Cha, W. Kim, X. Zhang *et al.*, *Polyaniline/graphene-functionalized flexible waste mask sensors for ammonia and volatile sulfur compound monitoring*, *ACS Appl. Mater. Interfaces* **14** (2022) 56056.
- [67] Y. Yan, X. Zhang, Y. Li, Y. Wang and J. Sun, *Conducting polymer-inorganic nanocomposite-based gas sensors: a review*, *Sci. Technol. Adv. Mater.* **21** (2020) 768.
- [68] S. Sharma, P. Sudhakara, A. A. B. Omran, J. Singh and R. A. Ilyas, *Recent trends and developments in conducting polymer nanocomposites for multifunctional applications*, *Polymers* **13** (2021) 2898.
- [69] C. V. Sudheep, A. Verma, P. Jasrotia, J. J. L. Hmar, R. Gupta, A. S. Verma *et al.*, *Revolutionizing gas sensors: The role of composite materials with conducting polymers and transition metal oxides*, *Results Chem.* **7** (2024) 101255.